Left–right dissociation of hippocampal memory processes in mice

Olivia A. Shipton[a,b], Mohamady El-Gaby[a], John Apergis-Schoute[c], Karl Deisseroth[d], David M. Bannerman[b,e], Ole Paulsen[a,b,1], and Michael M. Kohl[a,b,1]

[a]Department of Physiology, Development and Neuroscience, University of Cambridge, Cambridge CB2 3EG, United Kingdom; [b]OXION Initiative, Department of Physiology, Anatomy and Genetics, University of Oxford, Oxford OX1 3PT, United Kingdom; [c]Department of Pharmacology, University of Cambridge, Cambridge CB2 1PD, United Kingdom; [d]Department of Bioengineering, Stanford University, Stanford, CA 94305; and [e]Department of Experimental Psychology, University of Oxford, Oxford OX1 3UD, United Kingdom

Edited by Charles F. Stevens, The Salk Institute for Biological Studies, La Jolla, CA, and approved August 25, 2014 (received for review March 26, 2014)

Left–right asymmetries have likely evolved to make optimal use of bilaterian nervous systems; however, little is known about the synaptic and circuit mechanisms that support divergence of function between equivalent structures in each hemisphere. Here we examined whether lateralized hippocampal memory processing is present in mice, where hemispheric asymmetry at the CA3–CA1 pyramidal neuron synapse has recently been demonstrated, with different spine morphology, glutamate receptor content, and synaptic plasticity, depending on whether afferents originate in the left or right CA3. To address this question, we used optogenetics to acutely silence CA3 pyramidal neurons in either the left or right dorsal hippocampus while mice performed hippocampus-dependent memory tasks. We found that unilateral silencing of either the left or right CA3 was sufficient to impair short-term memory. However, a striking asymmetry emerged in long-term memory, wherein only left CA3 silencing impaired performance on an associative spatial long-term memory task, whereas right CA3 silencing had no effect. To explore whether synaptic properties intrinsic to the hippocampus might contribute to this left–right behavioral asymmetry, we investigated the expression of hippocampal long-term potentiation. Following the induction of long-term potentiation by high-frequency electrical stimulation, synapses between CA3 and CA1 pyramidal neurons were strengthened only when presynaptic input originated in the left CA3, confirming an asymmetry in synaptic properties. The dissociation of hippocampal long-term memory function between hemispheres suggests that memory is routed via distinct left–right pathways within the mouse hippocampus, and provides a promising approach to help elucidate the synaptic basis of long-term memory.

Unilateral specializations may facilitate greater processing power in bilateral brain structures by using the available neuronal circuitry more effectively. Nevertheless, the nature of the mechanisms that can act within the confines of duplicate neural structures to support different cognitive functions in each hemisphere remains elusive.

The hippocampus is essential for certain forms of learning and memory, both in humans (1) and in rodents (2, 3), and also plays an important role in navigation (4). The left and right mammalian hippocampi comprise the same anatomical areas and directional connectivity, and yet in the human hippocampus, task-related activity may be localized to only one hemisphere (5). This lateralization may enable the left and right hippocampus to support complementary functions in human episodic memory, with left hippocampal activity associated with an egocentric, sequential representation of space but greater activity in the right hippocampus when an allocentric representation is used (6). It has been suggested that human hippocampal asymmetry is primarily dictated by external asymmetry—namely, the left hemispheric involvement in language processing and the stronger contribution of the right hemisphere to visuospatial attention (7), supported by observations of left hippocampal dominance when semantic information is most task-relevant, compared with right hippocampal dominance when spatial information becomes more pertinent (8). However, a seminal discovery in the mouse brain suggests that left–right asymmetry may actually be a fundamental property of the mammalian hippocampus: it was found that the postsynaptic spine morphology and receptor distribution in CA1 pyramidal neurons is determined by whether the presynaptic input originates in the left or right CA3 (9, 10). Specifically, apical CA1 postsynaptic spines receiving input from the left CA3 are primarily thin and rich in GluN2B subunit-containing NMDA receptors (NMDARs); in contrast, there is a higher proportion of mushroom-shaped spines receiving right CA3 projection, and these larger spines have a lower density of GluN2B subunit-containing NMDARs (9, 10). Interestingly, synaptic plasticity also shows hemispheric asymmetry: irrespective of the hemispheric location of the CA1 neuron, GluN2B NMDAR-requiring spike timing-dependent long-term potentiation (LTP) was induced at synapses where presynaptic input originates in the left CA3, but not in the right CA3 (11).

These left–right synaptic differences raise the question as to whether memory processing in mice, as in humans, might differ between the left and right hippocampus. Therefore, in this study, we asked whether acutely inactivating one part of the asymmetric CA3–CA1 network unilaterally would affect learning and memory differentially between hemispheres. To test this, we silenced excitatory cells of CA3 in either the left or the right hippocampus, and consequently also both their ipsilateral and

Significance

The hippocampus is implicated in memory and spatial navigation. In rodents, in which this bilateral brain structure has been studied extensively, the left and right hippocampi have generally been considered functionally equivalent. However, recent work has revealed unexpected asymmetries in the molecular and morphological characteristics of neuronal connections according to brain hemisphere. To investigate whether this left–right difference has implications for hippocampal function, we acutely inhibited activity in an area-specific and genetically-defined population of hippocampal neurons during various behavioral tasks. We found that silencing the CA3 area of the left hippocampus impaired associative spatial long-term memory, whereas the equivalent manipulation in the right hippocampus did not. Thus, our data show that hippocampal long-term memory processing is lateralized in mice.

Author contributions: O.A.S., K.D., D.M.B., O.P., and M.M.K. designed research; O.A.S., M.E., J.A.-S., and M.M.K. performed research; K.D. contributed new reagents/analytic tools; O.A.S., D.M.B., and M.M.K. analyzed data; and O.A.S., D.M.B., O.P., and M.M.K. wrote the paper.

The authors declare no conflict of interest.

This article is a PNAS Direct Submission.

Freely available online through the PNAS open access option.

[1]To whom correspondence may be addressed. Email: op210@cam.ac.uk or michael.kohl@dpag.ox.ac.uk.

This article contains supporting information online at www.pnas.org/lookup/suppl/doi:10.1073/pnas.1405648111/-/DCSupplemental.

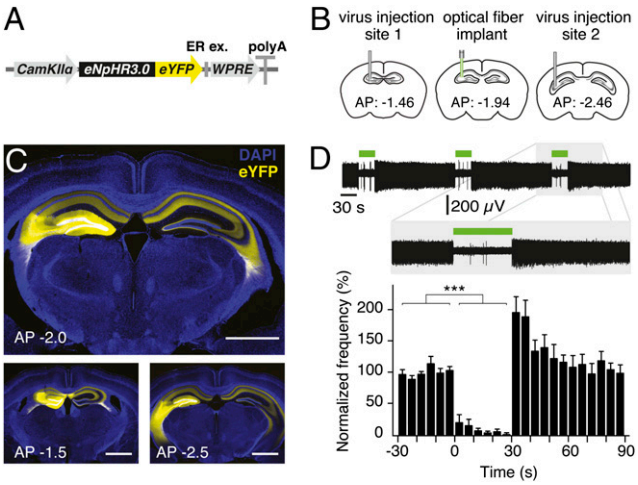

Fig. 1. Optogenetics enables acute silencing of CA3 activity in vivo. (*A*) Adeno-associated virus containing the eNpHR3.0-eYFP construct under the control of a CaMKIIα promoter was used. WPRE, woodchuck hepatitis post-transcriptional regulatory element. (*B*) Virus was unilaterally injected into two sites in the dorsal CA3 area of C57BL/6J mice for use in optrode recordings. For behavioral experiments, an optical fiber was also implanted between the two injection sites. (*C*) Two-site virus injection resulted in eNpHR3.0-eYFP or eYFP expression in CA3 and CA3 projections in the entire dorsal hippocampus. (*Upper*) Expression at approximate location of implant. (*Lower*) Approximate location of two injection sites. (Scale bars, 1 mm.) (*D*) Illumination of CA3 neurons in eNpHR3.0-expressing mice for 30 s resulted in a reversible reduction in spontaneous spiking frequency. A representative optrode recording trace as well as normalized mean frequency is shown. Error bars represent SEM.

contralateral projections to CA1, using the light-sensitive chloride pump halorhodopsin (eNpHR3.0) coexpressed with enhanced YFP (eYFP) (12).

Results

Halorhodopsin Permits Effective and Reversible Acute Silencing of Dorsal CA3 Neurons in Vivo. Injection of a viral construct containing eNpHR3.0 under control of the CaMKIIα promoter (AAV5-CaMKIIα-eNpHR3.0-eYFP) into two sites in the dorsal CA3 of either the left or right hippocampus in adult male wild-type mice gave robust expression of eNpHR3.0-eYFP throughout the dorsal CA3 (Fig. 1 *A*–*C*). We used optrode recordings in anesthetized mice to confirm that CA3 neurons in the dorsal hippocampus of eNpHR3.0-eYFP–expressing mice could be silenced by green light delivery for a duration equivalent to that of trials in the behavioral tasks; illumination was delivered via an optical fiber placed above the CA3 and in between the two injection sites. We found this method produced effective and reversible silencing of spontaneous spiking in single and multiunit recordings of CA3 neurons (Fig. 1*D*; light on: 8.6 ± 5.1% of baseline spiking levels, $P < 0.001$; 30–60 s after light on: 107 ± 12.7% of baseline spiking levels, $P = 0.612$; one-sample *t* tests compared with 100%; $n = 7$ recordings from two mice).

For behavioral testing, experimental mice received injections of AAV5-CaMKIIα-eNpHR3.0-eYFP into the two sites in the dorsal CA3 of one hemisphere that we had validated as effective with optrode recordings. A fiber-optic cannula was implanted between the two injection sites to illuminate expressing CA3 neurons (Fig. 1*B*). The efficacy of silencing was limited by the light spread rather than the virus expression because we used a low numerical aperture (0.22) fiber-optic cannula to illuminate only a subset of eNpHR3.0-expressing neurons (*SI Materials and Methods* and Fig. S1). Control mice received equivalent injections of a virus lacking eNpHR3.0 (AAV5-CaMKIIα-eYFP) and identical implant surgery to ensure that viral infection, surgery, and light delivery could not account for any behavioral differences; this gave two experimental groups of mice: left-NpHR and right-NpHR, with their respective control groups, left-YFP and right-YFP. We verified implant placement and the level of eYFP expression by immunohistochemistry after behavioral testing and confirmed that there were no significant differences in fiber placement in any of the three spatial dimensions (*SI Materials and Methods* and Fig. S2). All behavioral experiments and histology were performed with the experimenter blind to the identity of the mice.

Acute Silencing of Either Left or Right CA3 Impairs Hippocampus-Dependent Short-Term Memory. We first investigated whether acute unilateral CA3 silencing could affect short-term memory performance. Mice were tested on spontaneous alternation in a T-maze, which is a hippocampus-dependent short-term memory task that harnesses the strong novelty preference displayed by rodents (Fig. 2*A*) (13, 14). Each trial was self-contained, and mice received interleaved trials with and without light delivery; to achieve acute silencing, light was only delivered for the duration of each trial. All four groups showed equivalent levels of spontaneous alternation with the light off (left-NpHR = 82 ± 3%, right-NpHR = 85 ± 3%, left-YFP = 83 ± 2%, right-YFP = 86 ± 3%), indicating that there was no hemispheric asymmetry in the effect of surgery or tethering to the fiber-optic cable. However, with the light on, striking differences emerged between the groups of mice, indicating that left or right CA3 silencing impaired performance [Fig. 2*B*; left-NpHR = 22 mice, right-NpHR = 21 mice, left-YFP = 21 mice, right-YFP = 22 mice; two-way ANOVA; main effect of transgene: $F_{(1,82)} = 29.65$; $P < 0.001$ and a main

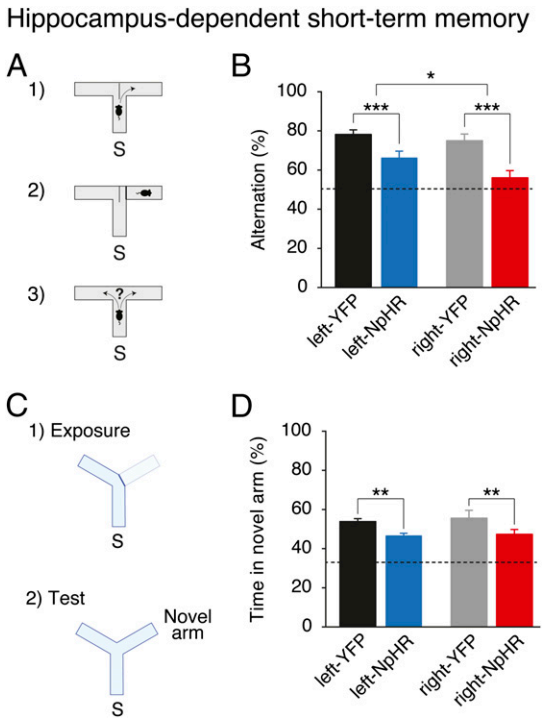

Fig. 2. Hippocampus-dependent short-term memory requires the left and right CA3. (*A*) Mice were tested on a spontaneous alternation task in a T-maze. S, start arm. (*B*) Light delivery during this task reduces spontaneous alternation of right-NpHR and left-NpHR mice compared with their respective YFP controls. (*C*) Mice were tested on a spatial novelty preference task in a Y-maze. (*D*) Light delivery during this task reduces preference for the novel arm in right-NpHR and left-NpHR mice compared with their respective YFP controls. Broken lines represent chance performance. Mean percentages ± SEM. *$P < 0.05$; **$P < 0.01$, ***$P < 0.001$.

effect of hemisphere: $F_{(1,82)} = 5.37$; $P = 0.023$, but no transgene by hemisphere interaction: $P = 0.23$].

We also tested mice on a different short-term memory task, the spatial novelty preference Y-maze task, in which extramaze spatial cues are important to generate novel arm preference (Fig. 2*C*) (15). The effect of light delivery was similar to that in the spontaneous alternation short-term memory task, with an impairment arising from unilateral CA3 silencing irrespective of whether it was the left or right CA3 that was silenced [Fig. 2*D*; left-NpHR = 6 mice, right-NpHR = 5 mice, left-YFP = 7 mice, right-YFP = 4 mice; two-way ANOVA; main effect of transgene: $F_{(1,18)} = 14.91$; $P = 0.001$].

Overall, these results show that a unilateral manipulation can impair hippocampus-dependent short-term memory, and that silencing of either the left or the right CA3 reduces performance on short-term memory tasks.

Acute Silencing of Left CA3 Impairs Hippocampus-Dependent Long-Term Memory, but Silencing the Right CA3 Has No Effect. We next wanted to investigate whether unilateral dorsal CA3 silencing could also impair hippocampus-dependent long-term memory. We tested the same mice on an appetitively motivated task where they had to learn which arm of an elevated Y-maze was rewarded using extramaze spatial cues. The rewarded location remained constant for each mouse across consecutive days of testing. We verified that this task generated a long-term memory of the rewarded arm because a separate cohort of mice showed stable performance upon retesting 1 wk after the end of the acquisition period with no exposure to the apparatus in the intervening period (83% correct choices on both last trial before and first trial after the 7-d retention interval; $n = 12$), which extended to the whole trial block (85 ± 6% correct arm choices on final block before retention interval and 85 ± 5% after retention interval; $n = 12$). A pseudorandom order of arm starts and periodic maze rotation between trials meant that intramaze cues provided no information that mice could use to perform the task successfully (Fig. 3*A*) (13, 16). Short-term memory errors could affect the acquisition of a spatial long-term memory task, but preventing arm reentry during a single trial removes this contribution to learning deficits (17). Therefore, to isolate long-term memory in this experiment, mice were only allowed to make one arm choice per trial and thus could not self-correct. Mice received blocks of 10 trials a day for 11 consecutive days, with five starts from the arm to the left of the designated rewarded arm, and 5 from the right in a pseudorandom order. Light was delivered for all mice during every trial, and was limited to the trial duration (10–40 s). To confirm that mice were not using olfactory cues from the reward to solve the task, the food was delivered after the arm choice was made on the final day of testing; this postchoice baiting did not cause performance to deteriorate.

Mice in the two control groups (left-YFP and right-YFP) acquired the task over the course of testing, reaching 90–100% accuracy. The right-NpHR group performed equivalent to the control mice. Strikingly, however, silencing the left CA3 did impair performance on this long-term memory task, and the deficit was not overcome even by the end of testing [Fig. 3 *B* and *C*; left-NpHR = 21 mice, right-NpHR = 19 mice, left-YFP = 18 mice, right-YFP = 22 mice; two-way ANOVA; main effect of transgene (NpHR/YFP): $F_{(1,76)} = 6.01$, $P = 0.017$; transgene by hemisphere interaction: $F_{(1,76)} = 11.46$, $P = 0.001$; analysis of simple main effects showed a significant effect of transgene on the left hemisphere: $F_{(1,76)} = 16.62$, $P < 0.001$ and a significant effect of hemisphere for NpHR: $F_{(1,76)} = 13.29$, $P < 0.001$]. The absence of an effect on task performance by silencing the right CA3 indicates that this network is dispensable for associative spatial long-term memory. Moreover, the acute nature of the manipulation, which limits compensatory changes associated with longer-term manipulations (18), further suggests the right CA3 is not required even under normal learning conditions. In contrast, the left CA3 appears to form an important part of the network that supports associative spatial long-term memory performance.

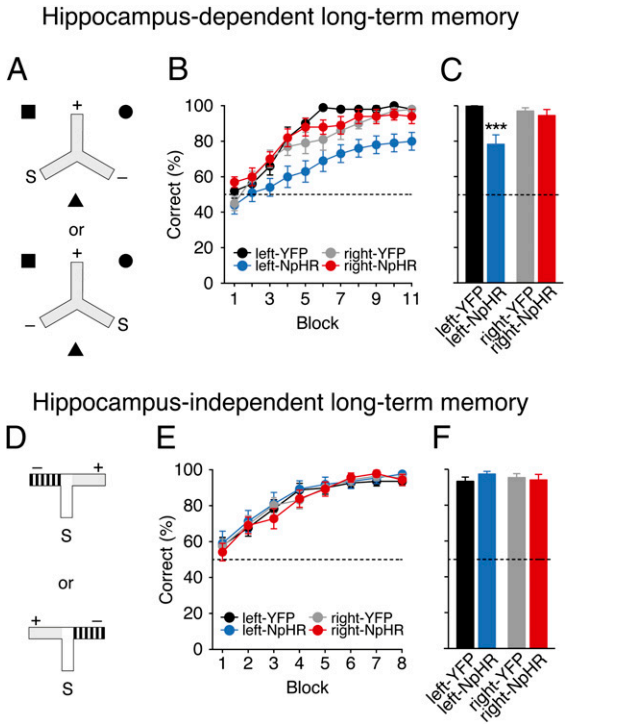

Fig. 3. Hippocampus-dependent associative spatial long-term memory uniquely requires the left CA3. (*A*) Mice were trained on a hippocampus-dependent long-term memory task where they had to associate a reward location that was fixed with respect to allocentric extramaze spatial cues (black square, circle, and triangle), and remained constant for each mouse across consecutive days of testing. Mice received arm starts (S) to the left or the right of the rewarded arm (+) in a pseudorandom order. Mice entering the nonrewarded arm (–) were not allowed to self-correct. (*B*) Light delivery in mice expressing eNpHR3.0 in the left CA3 (left-NpHR, blue) impairs but does not affect learning in right-NpHR mice (red) and control groups (left-YFP: black, right-YFP: gray) in this hippocampus-dependent long-term memory task. (*C*) Average performance on penultimate day. (*D*) Mice were trained on a hippocampus-independent visual-discrimination long-term memory task where they had to associate arm floor and wall color (gray vs. black-and-white stripes) with a reward; this was fixed for each mouse across consecutive days of testing. Rewarded (+) and nonrewarded (–) arms were pseudorandomly interchanged so that reward location was learnt independent of the spatial position of the arms of the maze. (*E*) Mice in all groups successfully learned this task at an equivalent rate. (*F*) Average performance on penultimate day. In both tasks, on the last day of testing, reward was delivered after the animal had chosen to control for the possibility of mice smelling the milk (postchoice baiting). Broken lines represent chance performance. Mean percentage correct choices ± SEM. ***$P < 0.001$.

Acute Silencing of Either Left or Right CA3 Does Not Affect Performance on a Hippocampus-Independent Visual (Nonspatial) Long-Term Memory Task. To ensure that unilateral optogenetic silencing does not cause a generalized sensorimotor or motivational behavioral impairment that could account for the deficit in the left-NpHR group on the spatial long-term memory task, a subset of the same mice, as well as a group of experimentally naïve mice, were trained on an associative, nonspatial visual discrimination T-maze task (16, 19) with trial-limited light delivery, as before (10–40 s). Mice had to learn to associate either a gray or a black/white-striped goal arm with reward (Fig. 3*D*). As with the previous long-term memory task, mice received training over consecutive days with 10 trials per block and were prevented from self-correcting within

a trial. However, in contrast to the associative spatial Y-maze task, the positions of the target arms were interchanged in a pseudo-random order so that, within each block, mice received a total of five starts with the rewarded arm to the left of the start arm and five starts with it to the right (Fig. 3*D*). Consequently, there was no extramaze spatial information that could be used to solve the task.

In contrast to the asymmetric effect of silencing on the spatial long-term memory task, all four groups of mice learnt this nonspatial control task successfully (90–100% correct) and at an equivalent rate [Fig. 3 *E* and *F*; left-NpHR = 15 mice, right-NpHR = 16 mice, left-YFP = 17 mice, right-YFP = 17 mice; two-way ANOVA; main effect of block: $F_{(7,427)} = 80.27$, $P < 0.001$, but no main effect of hemisphere: $F_{(1,161)} = 0.43$, $P = 0.51$, no main effect of transgene: $F_{(1,161)} = 0.09$, $P = 0.76$, no hemisphere by transgene interaction: $F_{(1,161)} = 0.43$, $P = 0.51$; and also no interaction between block and transgene $F_{(7,427)} = 0.19$, $P = 0.99$, nor between block and hemisphere: $F_{(7,427)} = 1.14$, $P = 0.34$ and no triple interaction: $F_{(7,427)} = 0.36$, $P = 0.93$]. Thus, the effect of optogenetic manipulation of the CA3 is limited to hippocampus-dependent tasks; furthermore, it implies that the impairment in the left-NpHR group during the associative spatial long-term memory task was not due a gross asymmetric disruption of sensorimotor or motivational aspects of task performance as a result of silencing of the left CA3.

High Frequency Stimulation-Induced LTP Is Present at CA3–CA1 Synapses Where Afferents Originate in the Left CA3, but Not in the Right CA3. Although their precise roles are debated, NMDAR-dependent synaptic plasticity processes are likely to be involved during performance on hippocampus-dependent spatial memory tasks (20–23). It has previously been reported that there is an asymmetry in the induction of hippocampal spike timing-dependent LTP (tLTP), such that tLTP can only be induced in CA3–CA1 synapses where the presynaptic input originates in the left CA3 via a GluN2B-dependent mechanism (11). However, conventional high-frequency stimulation (HFS)-induced LTP is not blocked by pharmacological GluN2B antagonism (24). Here we investigated whether the expression of HFS-LTP might also be asymmetric. Because hippocampal pyramidal neurons could not be driven at 100 Hz with optogenetic tools, we induced LTP with nonselective electrical HFS and sampled the left and right CA3–CA1 synapses selectively with optical stimulation to monitor any changes in synaptic weights.

Adult male wild-type mice were injected in the CA3 of one hemisphere with a viral construct containing channelrhodopsin-2 (hChR2) under control of the CaMKIIα promoter [AAV5-CaMKIIα-hChR2(E123T/T159C)-eYFP; Fig. 4*A*]. At 4–6 wk later, coronal slices were prepared for plasticity experiments, which were performed blind to injection side. We performed field recordings from CA1 with one electrically and one optically stimulated input pathway, and maximized the overlap between these two pathways by electrode and optical fiber placement (Fig. 4*A*). We recorded a stable baseline of both optically and electrically stimulated field excitatory postsynaptic potentials (fEPSPs), then induced LTP with high-frequency electrical stimulation (100 stimuli at 100 Hz). Following this induction protocol, we monitored the optical and electrical pathways to determine whether there was a difference in the response of synapses receiving input from either the left or right CA3. Despite equivalent potentiation in the electrical pathway in both left- and right-injected mice (left: 154 ± 6%, $n = 14$; right: 149 ± 6%, $n = 11$; $P = 0.50$), the optical pathway showed a significant increase in synaptic strength only in left-injected mice, irrespective of whether the slice was ipsilateral or contralateral to the injection side, and the fEPSP increase was significantly greater in left-injected compared with right-injected mice (Fig. 4 *B* and *C*; left: 145 ± 7%; right: 113 ± 7%; $P = 0.004$). This result held when the change in the optical pathway was normalized to the magnitude of electrical LTP (left: 84 ± 11% of electrical; right: 19 ± 15%; $P = 0.002$). Thus, the expression of HFS-LTP depends on whether the input originates in the left or right CA3; this suggests that these two inputs may perform different functions in vivo and provides one possible mechanistic explanation for the observed functional lateralization in long-term memory.

Discussion

Using trial-limited optogenetic silencing of excitatory neurons in either the left or right CA3, we have found a left–right functional dissociation in hippocampal memory performance in the mouse. Silencing of the left CA3 alone impairs performance on

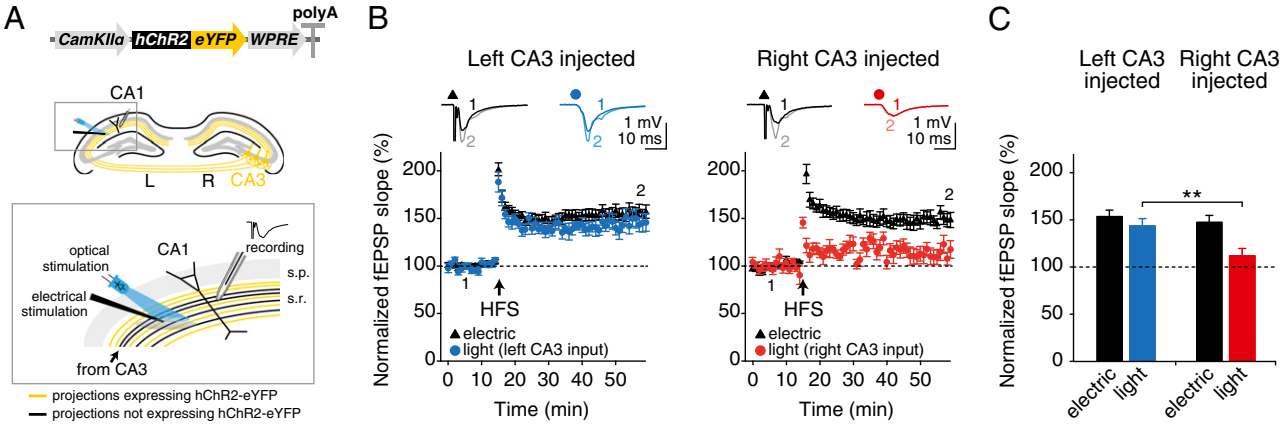

Fig. 4. High-frequency stimulation-induced LTP is asymmetrically expressed at the CA3–CA1 pyramidal cell synapse. (*A*, *Upper*) Adeno-associated virus containing hChR2-eYFP construct under the control of a CaMKIIα promoter was unilaterally injected into the dorsal CA3 area of C57BL/6J mice. (*Lower*) An electrode to deliver nonselective electrical stimulation was placed in the stratum radiatum and a high-power 470-nm LED was arranged to recruit an overlapping population of projections. Optical stimulation only recruits projections originating in the CA3 of the injected hemisphere (yellow), whereas electrical stimulation is nonselective (black and yellow). Electrical stimulation was used to deliver the high-frequency LTP induction protocol and the effects were monitored via field recording of EPSPs evoked by electrical or optical stimulation. (*B*) HFS produces robust LTP in the electrical pathway (black triangles), but LTP is only expressed in the optical pathway (circles) when projections originate in the left CA3. (*Insets*) Representative field EPSPs at the indicated time points (1, 2). (*C*) Significantly more LTP is observed in left-injected mice than in right-injected mice in the optical pathway. Broken lines represent baseline. Error bars represent SEM. $^{**}P < 0.01$, Student's *t* test.

a hippocampus-dependent long-term memory task. In contrast, unilateral silencing of either the left or the right CA3 causes a short-term memory deficit on hippocampus-dependent tasks. Together, these results show that there is a dissociation between the hemispheric involvement in short-term memory and long-term memory. We also found that high-frequency stimulation-induced LTP is only expressed at CA3–CA1 synapses when presynaptic input originates in the left CA3.

Unilateral hippocampal lesions in mice have not revealed a distinct hemispheric contribution to long-term memory (25), although split-brain mice with left eye deprivation showed greater spatial memory accuracy than those with right eye deprivation when the environmental complexity increased (26). Studies in rats have either shown no effect of unilateral lesions (27, 28) or no asymmetry of hippocampal function (27, 29), or have produced inconsistent findings (30–32). However, the chronic nature of surgical, and even pharmacological, manipulations can allow compensatory changes to develop. Acute optogenetic silencing can circumvent such adaption, which may explain why our unilateral silencing of a relatively small volume of cells in the mouse hippocampus produced considerable memory deficits; nevertheless, there may also be a larger indirect silencing effect from our manipulation at the CA3 network level, given its recurrent connectivity.

Optogenetic manipulations can provide new insights into the networks normally engaged during memory tasks (18), and thus enable a precise dissection of the functional roles of the areas within the hippocampus. Here we have found that the left CA3 is a key component in the hippocampal circuitry that supports long-term memory. Synaptic plasticity has been proposed as a cellular model for learning and memory (21), and it is likely that LTP or other NMDAR-dependent processes are important for accurate performance on spatial long-term memory tasks, although a causal relationship remains elusive. Therefore, it is tempting to speculate that the functional asymmetry relates to the synaptic asymmetry in the mouse hippocampus; CA3–CA1 synapses originating in the left CA3 have a high density of postsynaptic GluN2B subunit-containing NMDARs and show LTP, whereas CA1 spines that receive right CA3 input have a low density of GluN2B subunits, and do not exhibit LTP (9–11). In support of the interpretation that plastic synapses typical of left CA3–CA1 are required, a mutant mouse line that lacks synaptic asymmetry (homozygous *inversus viscerum* mice), instead having only synapses characteristic of those receiving right CA3 input in wild-types (33), is impaired on hippocampus-dependent short- and long-term memory tasks relative to heterozygous controls (34), whereas overexpression of GluN2B enhances LTP and improves hippocampus-dependent memory performance (35). Thus, our findings could be accounted for by a hippocampus-intrinsic mechanism, whereby these two types of synapse receive equivalent information but perform distinct information processing or storage functions. Our manipulation affects both the ipsilateral and contralateral CA3–CA1 projections originating in one hemisphere; although both ipsilateral and contralateral projections do show equivalent LTP in rats (36) and mice (11), we currently cannot exclude the possibility that they play independent roles. It is also conceivable that the asymmetry in long-term memory is explained either completely or in part because the left and right CA3 receive different information, akin to how the distinct functional contributions of dorsal and ventral hippocampus might arise through differences in first- and second-order inputs (37). One possible source of asymmetry before the hippocampus might be the lateral entorhinal cortex (LEC) input to dorsal hippocampus; the left LEC exhibits a higher metabolic demand than the right LEC (38), which may be indicative of distinct computational demands present in the neuronal circuitry. Asymmetry may even exist at the level of sensory inputs (30). These explanations are not mutually exclusive, however, because the different types of synapses receiving left compared with right CA3 input may have evolved in concert with such nonhippocampal asymmetries to optimally process different types of incoming information.

In contrast to the unique requirement for the left CA3 in a long-term memory task, unilateral silencing of the CA3 in either hemisphere was sufficient to impair hippocampus-dependent short-term memory. Thus, left CA3 silencing is not always more disruptive to hippocampal function than right CA3 silencing, which rules out trivial surgical or technical explanations for the left-NpHR deficit on the hippocampus-dependent long-term memory task, a conclusion supported by the equivalent implant placements between behavioral groups. This result further suggests that asymmetry does not arise from a different efficacy of silencing between hemispheres. Moreover, it corroborates the supposition that mechanisms supporting short- and long-term memory are dissociable (23). The reason why left or right CA3 silencing can cause an impairment in short-term memory may be because short-term memory requires a higher proportion of the hippocampal circuitry for effective performance, or necessitates communication between the CA3 in each hemisphere. Alternatively, the same result could arise if the left and right CA3 play independent, but equally necessary, roles in the activity required for short-term memory. One such role could relate to gamma oscillations, which have been closely linked to short-term memory (39), and, interestingly, a left–right asymmetry of gamma power was recently reported in the CA1 of the rat hippocampus following environmental enrichment (40).

The functional division of labor in memory processes that we have uncovered in the mouse suggests there could be parallels with the hippocampal asymmetry found in humans. Thus, left–right human hippocampal differences may not be a simple reflection of the lateralization in language processing (41) but, instead, asymmetry could be a fundamental characteristic of mammalian hippocampal function. In humans, a higher level of lateralization is associated with increased cognitive performance (42). Thus, hippocampal asymmetry may have arisen early in evolution and has been maintained to facilitate more efficient use of bilateral neural substrates. Such asymmetry might enable the hippocampus to support functions both in memory and in navigation (43), and could provide a synaptic mechanism by which the two can interact to underlie spatial long-term memory performance.

Materials and Methods

We used a total of 138 male C57BL/6J mice in this study. All procedures were performed in accordance with UK Home Office Regulations and approved by the License Review Committee at the University of Cambridge. For detailed methods and experimental procedures, see *SI Materials and Methods*.

ACKNOWLEDGMENTS. We thank R. Deacon for advice on behavioral testing; I. Goshen, L. Gunaydin, and T. Davidson for optogenetic advice; G. W. Y. Ang for helpful discussion; and R. Jude Samulski and the University of North Carolina Vector Core for manufacture of viral constructs. This research was made possible by grants from Alzheimer's Research UK and the Biotechnology and Biological Sciences Research Council (BBSRC), and additionally supported by an OXION Wellcome Trust Prize Studentship (to O.A.S.), a BBSRC Studentship (to M.E.), and a Royal Society Travel Grant (to M.M.K.).

1. Squire LR, Zola-Morgan S (1991) The medial temporal lobe memory system. *Science* 253(5026):1380–1386.
2. Morris RG, Garrud P, Rawlins JN, O'Keefe J (1982) Place navigation impaired in rats with hippocampal lesions. *Nature* 297(5868):681–683.
3. Eichenbaum H, Sauvage M, Fortin N, Komorowski R, Lipton P (2012) Towards a functional organization of episodic memory in the medial temporal lobe. *Neurosci Biobehav Rev* 36(7):1597–1608.
4. O'Keefe J, Dostrovsky J (1971) The hippocampus as a spatial map. Preliminary evidence from unit activity in the freely-moving rat. *Brain Res* 34(1):171–175.
5. Squire LR, et al. (1992) Activation of the hippocampus in normal humans: a functional anatomical study of memory. *Proc Natl Acad Sci USA* 89(5):1837–1841.
6. Iglói K, Doeller CF, Berthoz A, Rondi-Reig L, Burgess N (2010) Lateralized human hippocampal activity predicts navigation based on sequence or place memory. *Proc Natl Acad Sci USA* 107(32):14466–14471.

7. Hutsler J, Galuske RAW (2003) Hemispheric asymmetries in cerebral cortical networks. *Trends Neurosci* 26(8):429–435.
8. Motley SE, Kirwan CB (2012) A parametric investigation of pattern separation processes in the medial temporal lobe. *J Neurosci* 32(38):13076–13085.
9. Kawakami R, et al. (2003) Asymmetrical allocation of NMDA receptor epsilon2 subunits in hippocampal circuitry. *Science* 300(5621):990–994.
10. Shinohara Y, et al. (2008) Left–right asymmetry of the hippocampal synapses with differential subunit allocation of glutamate receptors. *Proc Natl Acad Sci USA* 105(49): 19498–19503.
11. Kohl MM, et al. (2011) Hemisphere-specific optogenetic stimulation reveals left–right asymmetry of hippocampal plasticity. *Nat Neurosci* 14(11):1413–1415.
12. Gradinaru V, et al. (2010) Molecular and cellular approaches for diversifying and extending optogenetics. *Cell* 141(1):154–165.
13. Deacon RMJ, Bannerman DM, Kirby BP, Croucher A, Rawlins JNP (2002) Effects of cytotoxic hippocampal lesions in mice on a cognitive test battery. *Behav Brain Res* 133(1):57–68.
14. Deacon RMJ, Rawlins JNP (2006) T-maze alternation in the rodent. *Nat Protoc* 1(1): 7–12.
15. Sanderson DJ, et al. (2007) Deletion of glutamate receptor-A (GluR-A) AMPA receptor subunits impairs one-trial spatial memory. *Behav Neurosci* 121(3):559–569.
16. Reisel D, et al. (2002) Spatial memory dissociations in mice lacking GluR1. *Nat Neurosci* 5(9):868–873.
17. Schmitt WB, Deacon RMJ, Seeburg PH, Rawlins JNP, Bannerman DM (2003) A within-subjects, within-task demonstration of intact spatial reference memory and impaired spatial working memory in glutamate receptor-A-deficient mice. *J Neurosci* 23(9): 3953–3959.
18. Goshen I, et al. (2011) Dynamics of retrieval strategies for remote memories. *Cell* 147(3):678–689.
19. Lyon L, et al. (2011) Fractionation of spatial memory in GRM2/3 (mGlu2/mGlu3) double knockout mice reveals a role for group II metabotropic glutamate receptors at the interface between arousal and cognition. *Neuropsychopharmacology* 36(13): 2616–2628.
20. Bliss TV, Collingridge GL (1993) A synaptic model of memory: Long-term potentiation in the hippocampus. *Nature* 361(6407):31–39.
21. Martin SJ, Grimwood PD, Morris RG (2000) Synaptic plasticity and memory: An evaluation of the hypothesis. *Annu Rev Neurosci* 23:649–711.
22. Ramirez S, Tonegawa S, Liu X (2013) Identification and optogenetic manipulation of memory engrams in the hippocampus. *Front Behav Neurosci* 7:226.
23. Bannerman DM, et al. (2014) Hippocampal synaptic plasticity, spatial memory and anxiety. *Nat Rev Neurosci* 15(3):181–192.
24. Shipton OA, Paulsen O (2014) GluN2A and GluN2B subunit-containing NMDA receptors in hippocampal plasticity. *Philos Trans R Soc Lond B Biol Sci* 369(1633): 20130163.
25. Gerlai RT, McNamara A, Williams S, Phillips HS (2002) Hippocampal dysfunction and behavioral deficit in the water maze in mice: An unresolved issue? *Brain Res Bull* 57(1):3–9.
26. Shinohara Y, et al. (2012) Right-hemispheric dominance of spatial memory in split-brain mice. *Hippocampus* 22(2):117–121.
27. Li H, Matsumoto K, Watanabe H (1999) Different effects of unilateral and bilateral hippocampal lesions in rats on the performance of radial maze and odor-paired associate tasks. *Brain Res Bull* 48(1):113–119.
28. Jerman T, Kesner RP, Hunsaker MR (2006) Disconnection analysis of CA3 and DG in mediating encoding but not retrieval in a spatial maze learning task. *Learn Mem* 13(4):458–464.
29. Fenton AA, Bures J (1993) Place navigation in rats with unilateral tetrodotoxin inactivation of the dorsal hippocampus: Place but not procedural learning can be lateralized to one hippocampus. *Behav Neurosci* 107(4):552–564.
30. LaMendola NP, Bever TG (1997) Peripheral and cerebral asymmetries in the rat. *Science* 278(5337):483–486.
31. Poe GR, et al. (2000) Partial hippocampal inactivation: Effects on spatial memory performance in aged and young rats. *Behav Neurosci* 114(5):940–949.
32. Klur S, et al. (2009) Hippocampal-dependent spatial memory functions might be lateralized in rats: An approach combining gene expression profiling and reversible inactivation. *Hippocampus* 19(9):800–816.
33. Kawakami R, Dobi A, Shigemoto R, Ito I (2008) Right isomerism of the brain in *inversus viscerum* mutant mice. *PLoS ONE* 3(4):e1945.
34. Goto K, et al. (2010) Left–right asymmetry defect in the hippocampal circuitry impairs spatial learning and working memory in iv mice. *PLoS ONE* 5(11):e15468.
35. Tang YP, et al. (1999) Genetic enhancement of learning and memory in mice. *Nature* 401(6748):63–69.
36. Bliss TV, Lancaster B, Wheal HV (1983) Long-term potentiation in commissural and Schaffer projections to hippocampal CA1 cells: An in vivo study in the rat. *J Physiol* 341(1):617–626.
37. Ohara S, Sato S, Tsutsui K, Witter MP, Iijima T (2013) Organization of multisynaptic inputs to the dorsal and ventral dentate gyrus: Retrograde trans-synaptic tracing with rabies virus vector in the rat. *PLoS ONE* 8(11):e78928.
38. Khan UA, et al. (2014) Molecular drivers and cortical spread of lateral entorhinal cortex dysfunction in preclinical Alzheimer's disease. *Nat Neurosci* 17(2):304–311.
39. Fuchs EC, et al. (2007) Recruitment of parvalbumin-positive interneurons determines hippocampal function and associated behavior. *Neuron* 53(4):591–604.
40. Shinohara Y, Hosoya A, Hirase H (2013) Experience enhances gamma oscillations and interhemispheric asymmetry in the hippocampus. *Nat Commun* 4:1652.
41. Bishop DVM (2013) Cerebral asymmetry and language development: Cause, correlate, or consequence? *Science* 340(6138):1230531.
42. Gotts SJ, et al. (2013) Two distinct forms of functional lateralization in the human brain. *Proc Natl Acad Sci USA* 110(36):E3435–E3444.
43. Eichenbaum H, Cohen NJ (2014) Can we reconcile the declarative memory and spatial navigation views on hippocampal function? *Neuron* 83(4):764–770.

Supporting Information

Shipton et al. 10.1073/pnas.1405648111

SI Materials and Methods

Behavioral Experiments. ***Animals and adeno-associated virus vectors.*** All experiments were performed in accordance with UK Home Office Regulations and under personal and project licenses held by the authors. Male C57BL/6J mice (Charles River Laboratories or Harlan) were housed in polycarbonate cages of 5–10 mice on a 12-h light/dark cycle (7:00 AM–7:00 PM), and had access to food and water ad libitum, except when on food restriction during appetitively motivated behavioral tests. eNpHR3.0 was fused in-frame to enhanced YFP (eYFP) and driven by a CaMKIIα promoter (1). Adeno-associated viral (AAV) particles of serotype 5 were produced by the Vector Core Facility at The University of North Carolina at Chapel Hill (titers detailed below).

Surgery and light delivery. Mice (10–12 wk old) were anesthetized with 2–4% (vol/vol) isoflurane at 0.6–1.4 $L{\cdot}min^{-1}$, placed on a heating pad to aid body temperature maintenance and their head fixed in a stereotactic apparatus (Kopf Instruments). The head was leveled and three small craniotomies were made above either the left or right dorsal hippocampus. At sites 1 and 3 [site 1: anteriorposterior (AP): −1.46 mm, mediolateral (ML): ±1.25 mm, dorsoventral (DV): −2.00 mm; site 3: AP: −2.46 mm, ML: ± 2.40 mm, DV: −2.30, all coordinates from skull surface at bregma], 0.75-μL virus suspension (AAV5-CaMKIIα-eNpHR3.0-eYFP-WPREpA, 4×10^{12} viral molecules per milliliter for experimental mice and AAV5-CaMKIIα-eYFP, 6×10^{12} viral molecules per milliliter for control mice; University of North Carolina Vector Core) was delivered at a rate of 0.1 $\mu L{\cdot}min^{-1}$ through a 33-gauge needle using a Hamilton Microliter syringe. Following a 6-min wait after bolus injection, the needle was retracted by 0.20 mm and after another 4-min wait slowly retracted fully. At site 2 (AP: −1.94 mm, ML: ±2.00 mm), a fiber optic cannula [200 μm diameter, 0.22 N.A. (Doric Lenses)] was lowered to DV −1.80 mm (from bregma) and secured to the skull using dental cement (C&B Metabond; Prestige Dental and Simplex). The scalp incision was sutured, and anti-inflammatory and analgesic drugs (2 $mg{\cdot}kg^{-1}$ meloxicam; 0.1 $mg{\cdot}kg^{-1}$ buprenorphine) were administered s.c. to aid recovery.

Green laser light from a solid-state laser diode (532 nm, 24 ± 3 mW at fiber tip; Laser 2000) was collimated into an aperture-matched fiberoptic patch cord (Doric Lenses) that was connected to the fiberoptic implants.

To ensure strong eNpHR3.0 expression in an area of cells 0.5 mm away from each injection site, a relatively large quantity of virus was injected into each site in the CA3c subfield (0.75 μL, at a titer of $4–6 \times 10^{12}$ viral molecules per milliliter); this also produced virus expression in the dentate gyrus (DG), but additional specificity was achieved through the use of a low numerical aperture (0.22 N.A.) optical fiber to restrict light spread and manipulate a volume of cells between the two injection sites. The efficacy of this approach is illustrated by the restricted area of YFP photobleaching below the optical fiber (Fig. S1). A similar principle of limiting optogenetic silencing by spatially restricted light delivery has been used previously (2).

To provide a quantitative estimate of the degree of specificity of our optogenetic manipulation in the CA3 compared with DG, we used available experimental values from Yizhar et al. (3) for transmission of 594-nm wavelength light from a 0.37-N.A. fiber through brain tissue; this provided an upper limit of transmission because we used a lower wavelength light for behavior (532 nm), which penetrates less through tissue and also a lower N.A. fiber (0.22) that will cause a more restricted light cone (full acceptance angle is 25° for 0.22 N.A. compared with 46° for 0.37 N.A.). We determined the location of implants in each mouse (*Immunohistochemistry*; Fig. S2) and used these placements and the light spread data to estimate the proportion of light at 1%, 5%, 10%, and 50% (isobar lines) of the maximum light power (24 ± 3 mW at tip in our experiments) that reached the DG (Fig. S1) and calculated values of (mean ± SEM): 13 ± 3% DG overlap for 50% of total laser power; 16 ± 3% overlap for 10% total power; 15 ± 3% overlap for 5% total power; and 17 ± 2% for 1% of total power ($n = 86$).

To confirm that differences in implant placement, and hence the region exposed to light, between behavioral groups could not account for the difference in silencing left compared with right CA3 in spatial long-term memory, we recorded the average position of the tip of each fiber optic implant (mean ± SEM) shown in Fig. S2 (left-NpHR = 22 mice, right-NpHR = 21 mice, left-YFP = 21 mice, right-YFP = 22 mice): left-NpHR: AP: −2.11 ± 0.04 mm, ML: 1.98 ± 0.03 mm, DV: −1.64 ± 0.05 mm; right-NpHR: AP: −2.12 ± 0.07 mm, ML: 1.87 ± 0.06 mm, DV: −1.65 ± 0.04 mm; left-YFP: AP: −2.06 ± 0.06 mm, ML: 1.94 ± 0.05 mm, DV: −1.63 ± 0.06 mm; right-YFP: AP: −2.21 ± 0.07 mm, ML: 2.01 ± 0.06 mm, DV: −1.75 ± 0.04 mm.

There were no significant differences between the NpHR experimental groups in average optical fiber placement in any spatial dimension that could explain the asymmetry in long-term memory [left-NpHR = 22 mice, right-NpHR = 21 mice; two-way ANOVA with spatial dimension (AP, ML, DV) as a within-subjects factor and hemisphere as a between-subjects factor: no main effect of hemisphere $F_{(1,41)} = 2.26$, $P = 0.141$; and no hemisphere by spatial dimension interaction $F_{(2,82)} = 0.503$, $P = 0.607$].

Optrode recordings. Adult male mice received dual injections of AAV5-CaMKIIα–driven eNpHR3.0 at sites 1 and 3 as described above, but without the fiberoptic implant. Following at least 8 wk for expression to develop, mice were anesthetized with i.p. injections of urethane ($1.2\ g{\cdot}kg^{-1}$), ketamine ($100\ mg{\cdot}kg^{-1}$), and xylazine ($10\ mg{\cdot}kg^{-1}$). Simultaneous optical stimulation and electrical recording in CA3 were carried out as described previously (4) using an optrode consisting of an extracellular parylene-C insulated tungsten microelectrode (127-μm diameter, 1 MΩ; A-M Systems) tightly bundled with an optical fiber (200 μm, 0.22 N.A.; Thorlabs), with the tip of the electrode protruding 0.5–0.7 mm beyond the fiber end to ensure illumination of the recorded neurons. The optical fiber was coupled to the laser and light output adjusted to 20–25 mW at the fiber tip. The optrode was initially placed above CA3 (AP: −1.94 mm, ML: ±2.00 mm, DV: −1.80 mm; equivalent to the implant coordinates) and gradually lowered in 0.1-mm increments. Signals were recorded and bandpass-filtered between 300 Hz and 5 kHz using a microelectrode amplifier (1800 Microelectrode AC Amplifier; A-M Systems) and recorded with Spike2 (Cambridge Electronic Design). A baseline of 1 min was recorded when clear spikes were detected, followed by 30-s continuous laser light illumination and then at least 1 min recording without light. This process was then repeated up to four times.

Behavioral testing. Following at least 8 wk for expression of eNpHR3.0-eYFP or eYFP to develop after surgery, mice were handled to habituate them to the experimenter and accustom them to connection of the implant to the fiber-optic cable. All behavioral testing was done during the light phase of the light/dark cycle and with the experimenter blind to condition. All mice were used first in the spontaneous alternation T-maze task and then in the appetitive Y-maze task. The last batch of 36 mice was additionally used in the visual discrimination T-maze task and

supplemented by a group of experimentally naïve mice. The latter group of mice then went on to be tested in the novelty preference Y-maze task. Any mice that lost implants during testing were perfused (*Immunohistochemistry*) and excluded from any tasks they did not complete.

Spontaneous alternation short-term memory T-maze task. The T-maze was black painted wood and had two sliding doors to enclose the two choice arms (30 × 10 cm, 20-cm high walls) and a removable central barrier (extending 5 cm into central arm). During each trial, the floor was covered with wood chipping litter. Mice received two self-contained trials each day, one in the morning and one in the afternoon. Mice were started in a pseudorandom order within the cage, which varied across trials. Before the start of each trial, the implant was connected to the laser. For "light on" trials, the illumination was started before the mouse was placed in the maze and light was then on continuously during the trial; light was turned off once the mouse was removed from the maze at the end of the trial. "Light off" trials were pseudorandomly interleaved, during which mice were still connected to the laser but no light was delivered. Mice were started facing outward and given a free choice of arm. The central barrier was in position so mice received sensory input from only the chosen side before they could enter the arm. Once they had entered an arm, a black painted wooden block was positioned so they experienced a 30-s exploratory period in their chosen arm. The central barrier was removed, and then the mouse was removed from the explored arm and immediately replaced in the start arm facing outward. The subsequent arm choice was recorded, and if it was the novel one, this was scored as a correct alternation. Because it has been reported that delay times can affect performance on short-term memory tasks (5), if mice had not made an arm decision after 20 s in the second phase of the trial, the trial was aborted.

Spatial novelty preference short-term memory Y-maze task. The novelty preference Y-maze consisted of three transparent colorless Perspex arms (8 cm wide and 25 cm tall) mounted onto a painted white wooden board. During each trial, the floor was covered with wood chipping litter. Each arm could be closed off with a block made of opaque Perspex. Mice were assigned a novel arm and a start arm (in relation to fixed extramaze cues). Arm designations were counterbalanced such that approximately equal proportions of each experimental group were assigned to each novel arm. During the first exploration phase of the trial, the novel arm was blocked off. Mice were placed facing outward in the start arm, and were given 5 min to explore the start and other arms. Timing was started once the mouse left the start arm. Before being placed in the maze, the implant was connected to the laser and illumination started; light was then on continuously during the first part of the trial. The light was turned off once the mouse was removed from the maze and the implant disconnected. Mice were then placed back in their home cage for 1 min. The arm block was then removed and wood chipping shuffled. Mice were reconnected to the laser and illumination started, light was then on continuously during the second part of the trial. Mice were then placed back in the start arm facing outward and given 2 min to explore all three arms; the time spent in each arm was recorded. Timing started once the mouse left the start arm. Mice received two separate novelty preference tests, 2–4 d apart, each in a different room.

Spatial long-term memory Y-maze task. The elevated Y-maze was constructed of gray painted wooden arms (50 × 13 cm bordered by 1-cm-high white plastic walls), extending from a central triangular platform. Metal food wells (1.5 cm high) were positioned 5 cm from the distal end of the arms. The maze was elevated 82 cm from the floor. Mice were put on a restricted feeding schedule, allowing them to maintain at least 85% of their free-feeding body weight. Mice were introduced to the food reward (0.1 mL of sweetened condensed milk diluted 50:50 with water) in their home cages to overcome neophobia and then pretrained on the elevated Y-maze in a room different to where behavioral testing would occur until they were highly motivated to search for food and running freely on the Y-maze (reaching the food reward in under 15 s for three consecutive trials). Mice were assigned a rewarded target arm (designated A, B, or C according to its fixed position relative to allocentric extramaze spatial cues). Target arm designations were counterbalanced such that approximately equal proportions of each experimental group were assigned to each arm. Mice were started facing outward in either the left or right arm relative to the target arm and received 10 trials per day for 11 consecutive days. On each day, mice had five starts from the left of the target arm and five starts from the right in a pseudorandom order with no more than three consecutive starts from the left or right. Mice were started in a pseudorandom order within the cage, which varied across trials, and the intertrial interval (ITI) was ∼15 min. Before being placed on the maze, the implant was connected to the laser and illumination started; light was then on continuously during the trial and was turned off once the mouse was removed from the maze (trial duration 10–40 s). If a mouse made the correct choice, it was allowed to consume the reward, but the trial was ended if mice chose the incorrect arm and after they had seen the empty food well (i.e., they were not allowed to self-correct). The maze was pseudorandomly rotated either clockwise or anticlockwise between trials to ensure that olfactory, tactile, or visual cues on the maze itself (intramaze cues) did not provide information that could be used to solve the task. On the last day of testing, food was only delivered once the mouse reached the food well to check that mice did not use reward odor to solve the task (postchoice baiting). When not performing the task, mice were kept behind a screen to minimize exposure to the testing room and cues in the absence of laser light. A subset of mice was tested for longer-term memory recall for the goal location. These mice were trained in the Y-maze task for 11 d, as described above; they then received a 7-d period with no testing, before receiving a further block of 10 trials. These 10 trials were conducted on one day in the same room as previously, with identical cues and the same arm being rewarded.

Visual discrimination long-term memory T-maze task. The visual T-maze consisted of two painted wooden interchangeable arms, one gray and one black-and-white striped (30 × 10 cm, 30-cm-high walls). The starting arm, central area, and back wall were all brown. Mice were put on a restricted feeding schedule, allowing them to maintain at least 85% of their free-feeding body weight, and were reintroduced to the food reward (0.1 mL of sweetened condensed milk diluted 50:50 with water). Mice were assigned a target arm (with numbers trained to the gray or striped arm counterbalanced across each experimental group). Before testing commenced, mice received four forced pretrials to overcome any potential neophobia to the goal arms. In these forced trials, one arm was blocked off so that they experienced each possible combination across the four trials (gray-left, gray-right, striped-left, and striped-right), and the reward contingencies applied as they would for the rest of the experiment. For training, mice received 10 trials per day for 8 consecutive days and were always started facing outward in the central arm, which remained in a fixed position. To ensure that there was no spatial solution to the task, the gray and the striped arm were interchanged such that each day mice received five trials where the rewarded arm was on the left and five where it was on the right. Reward arm location was in a pseudorandom order with no more than three consecutive positions of the rewarded arm being the same. Mice were started in a pseudorandom order within the cage, which varied across trials, and the ITI was ∼15 min. Before being placed in the maze, the implant was connected to the laser and illumination started; light was then on continuously during the trial. The light was turned off once the mouse was removed

from the maze. If a mouse made the correct choice, it was allowed to consume the reward, but if an incorrect choice was made the mouse was removed from the maze immediately after they had seen the empty food well, analogous to the appetitive Y-maze task. On the last day of testing, food was only delivered once the mouse reached the food well to check that mice did not use reward odor to solve the task (postchoice baiting).

Immunohistochemistry. Mice were anesthetized by i.p. injection of pentobarbital (533 $mg \cdot kg^{-1}$) and then transcardially perfused with cold PBS (pH 7.4) followed by 4% (wt/vol) paraformaldehyde (PFA) in PBS. Brains were postfixed for 36 h at 4 °C in PFA in PBS, then rinsed and subsequently infiltrated with 30% (wt/vol) sucrose in PBS for at least 48 h. Coronal sections of 40-μm thickness along the entire dorsal–ventral axis of the hippocampus were cut using a microtome (Spencer Lens Co.) and divided into three series. The first series was immunostained to visualize expression of the YFP tag. Sections were rinsed for 3 × 10 min in PBS and incubated for 1 h in PBS with 0.2% (wt/vol) Triton X-100 (PBS-T) containing 1% (wt/vol) bovine serum (Sigma); they were then incubated for 15 h at 4 °C in PBS-T containing 1% bovine serum and anti-GFP (goat, 1:1,000; Abcam, ab5450). The sections were then rinsed for 3 × 10 min in PBS and incubated in PBS-T containing 1% bovine serum and Alexa 488-labeled secondary antibody (donkey anti-goat; 1:1,000; Invitrogen, A11055) for 90 min at room temperature. After three 10-min rinses in PBS, slices were mounted in VectaShield (Vector Labs). Fluorescence images (Zeiss Axioskop 2 microscope) were taken either following the protocol for YFP immunostaining described above (first batch of mice) or using the intrinsic fluorescence of YFP (subsequent batches) and scored blindly for the presence of expression. Brightfield images (Zeiss Axioskop 2 microscope) were also taken and scored blindly for implant location (Fig. S2).

Data analysis. Optrode recording data were analyzed using Spike2; a voltage threshold was set and spike templates were produced during the baseline in Spike2 and counted. Data were then binned (5 s) and normalized to a 30-s baseline. The normalized means during silencing were compared with 100% using a one-sample *t* test. The behavioral results were analyzed by two-way ANOVA with between-subjects factors of transgene (NpHR vs. YFP) and hemisphere (left vs. right), and also a within-subjects factor of block for the long-term memory tests. Significant interactions were explored by analysis of simple main effects. *N* numbers (unless otherwise stated) refer to the number of mice.

Electrophysiology Experiments. ***Animals and AAVs.*** All experiments were performed in accordance with UK Home Office Regulations and under personal and project licenses held by the authors. Male C57BL/6J mice (Charles River Laboratories) were housed in polycarbonate cages of 5–10 mice on a 12-h light/dark cycle, and had access to food and water ad libitum. hChR2(E123T/T159C) was fused in-frame to eYFP and driven by a CaMKIIα promoter. Adeno-associated viral particles of serotype 5 were produced by the Vector Core Facility at the University of North Carolina at Chapel Hill.

Virus injections. Wild-type mice (14–16 wk old) were anesthetized with 2–4% (vol/vol) isoflurane at 0.6–1.4 $L \cdot min^{-1}$. Using a stereotactic apparatus (Kopf Instruments), a small craniotomy was made 2.3 mm anterior and 2.2 mm lateral (either left or right) from bregma. Through a small durotomy, 0.6-μL virus suspension (AAV5-CaMKII-hChR2(E123T/T159C)-eYFP, 4×10^{12} viral molecules per milliliter; University of North Carolina Vector Core) was delivered at a rate of 0.1 $\mu L \cdot min^{-1}$ 2.25 mm below the skull surface through a 33-gauge needle using a Hamilton Microliter syringe. Following a 5-min wait after bolus injection, the needle was retracted by 0.2 mm and after another 5-min wait slowly retracted fully. The scalp incision was sutured, and postinjection analgesic (0.03 $mg \cdot kg^{-1}$ buprenorphine) was administered i.p. to aid recovery.

Slice preparation. Coronal hippocampal slices (350 μm) were prepared after decapitation under deep isoflurane-induced anesthesia. After dissection in ice-cold artificial cerebrospinal fluid (ACSF) containing (mM): NaCl 126; KCl 3; NaH_2PO_4 1.25; $MgSO_4$ 2; $CaCl_2$ 2; $NaHCO_3$ 25; glucose 10; pH 7.2–7.4; bubbled with carbogen gas (95% O_2, 5% CO_2), slices were maintained at room temperature (22–25 °C) in a submerged-style holding chamber for at least 1 h. For recording, slices were transferred to an interface-style recording chamber maintained at 31–33 °C superfused with ACSF at a rate of 0.5 $mL \cdot min^{-1}$; recording started at least 10 min after the slices were transferred.

Electrophysiological protocols and light delivery. Extracellular field recordings from CA1 were made with an Axoclamp-2A amplifier in bridge mode, and data acquired with an InstruTech ITC-16 A/D board (InstruTech Corp.) using Igor Pro software (WaveMetrics). Borosilicate glass recording electrodes were filled with ACSF. Recording and stimulation electrodes were positioned in the stratum radiatum of CA1. The optical fiber was also placed in the stratum radiatum, as close as possible to the stimulation electrode to ensure maximal overlap of fibers recruited. Synaptic efficacy was monitored by alternately stimulating the Schaffer collaterals at 0.2 Hz (50 μs, 30–150 μA) with a 2-MΩ monopolar tungsten electrode (A-M Systems) connected to a stimulus isolator unit (ISO-Flex; A.M.P.I.) for the electrical pathway and by stimulating at 0.2 Hz (5 ms, 0.5–1.2 A) using a 200-μm diameter, 0.39-N.A. optical fiber (Thorlabs) connected to a blue (470 nm) fiber-coupled high-power LED (Thorlabs) for the optical pathway. Stimulation strength was set to elicit a field excitatory postsynaptic potential (fEPSP) of half-maximal amplitude. fEPSP slopes were monitored for a baseline period of at least 15 min. If synaptic transmission was stable (<15% change in fEPSP slopes over 15 min), the Schaffer collateral pathway was stimulated with a single high-frequency tetanus (100 Hz for 1 s, 100 μs) in the electrical pathway. The level of overlap between the optical and the electrical pathways was estimated using linear summation. Linear summation (LS) was measured by stimulating the electrical and optical pathways independently at the stimulation strength used for the LTP recording. Both optical and electrical pathways were then triggered simultaneously and the amplitude of the resulting fEPSP measured. The degree of linear summation was quantified as

$$\frac{(optical\ \ fEPSP\ \ amplitude + electrical\ \ fEPSP\ \ amplitude) - simultaneous\ \ fEPSP\ \ amplitude}{optical\ \ fEPSP\ \ amplitude},$$

whereby an overlap index of 0 would suggest no overlap, and 1 would suggest complete overlap. The optical fEPSP amplitude was used as the normalization factor to estimate the fraction of the optical fEPSP that was stimulated by the electrical pathway. This linear summation measure was found not to differ between right- and left-injected mice (LS left: 0.47 ± 0.10, $n = 10$; LS right: 0.40 ± 0.09, $n = 11$; $P = 0.602$, Student *t* test).

Data analysis. Changes in synaptic efficacy were estimated by using the mean fEPSP slopes of 30–45 min after tetanic stimulation

normalized to the mean fEPSP slope during the last 5 min of baseline recording. All analysis was done with Igor Pro. Statistical analysis was performed using SPSS software. All values are given as mean ± SEM, and statistical significance was assessed using Student's two-tailed *t* test. Numbers (*N*) refer to the number of slices, with each condition obtained from at least six animals. All field recording experiments in Fig. 4 were performed with the experimenter blind to injection side. Data from left- and right-injected mice was collected using slices both ipsilateral and contralateral to the injection site. However, because there was no difference in the magnitudes of electrical and optical LTP between slices recorded ipsilaterally or contralaterally to the injection site, as has also been found previously for timing-dependent LTP (6), the results were pooled.

1. Gradinaru V, et al. (2010) Molecular and cellular approaches for diversifying and extending optogenetics. *Cell* 141(1):154–165.
2. Tye KM, et al. (2011) Amygdala circuitry mediating reversible and bidirectional control of anxiety. *Nature* 471(7338):358–362.
3. Yizhar O, Fenno LE, Davidson TJ, Mogri M, Deisseroth K (2011) Optogenetics in neural systems. *Neuron* 71(1):9–34.
4. Gradinaru V, et al. (2007) Targeting and readout strategies for fast optical neural control in vitro and in vivo. *J Neurosci* 27(52):14231–14238.
5. Zhang X-H, Liu S-S, Yi F, Zhuo M, Li B-M (2013) Delay-dependent impairment of spatial working memory with inhibition of NR2B-containing NMDA receptors in hippocampal CA1 region of rats. *Mol Brain* 6:13.
6. Kohl MM, et al. (2011) Hemisphere-specific optogenetic stimulation reveals left–right asymmetry of hippocampal plasticity. *Nat Neurosci* 14(11):1413–1415.

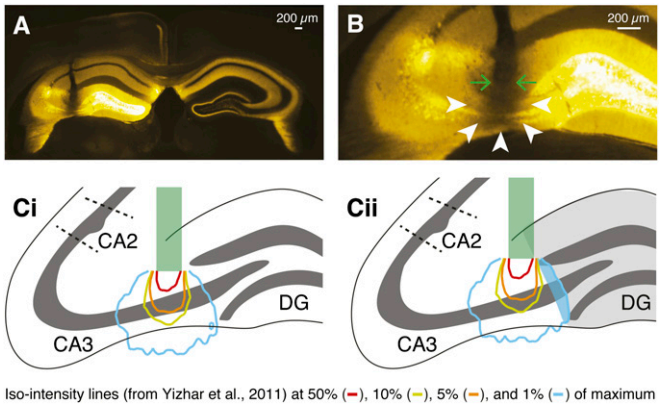

Fig. S1. Limiting optogenetic silencing to the CA3 area by spatially restricted light delivery. (*A* and *B*) Photobleaching in a YFP-expressing control mouse following 532-nm light delivery from a 0.22-N.A. fiber optic implant. (*A*) Coronal section through the dorsal hippocampus showing the optical fiber tract in one hippocampus and bleached area in CA3 following light delivery. (*B*) Close-up of *A*: green arrows indicate tip location of the fiber optic implant, white arrowheads point at bleaching due to light delivery. (*Ci*) Schematic of the hippocampus with superimposed fiber optic implant in green and isointensity lines from Yizhar et al. (3) illustrating how 594-nm light passes through brain tissue from a 0.37-N.A. optical fiber. (*Cii*) To obtain a conservative approximation for the specificity of the manipulation, the proportion of light at a percentage of total power at the tip that entered the dentate gyrus (light gray shaded zone labeled DG) was calculated using these isointensity lines. For this implant placement, the light blue shaded region represents the proportion of light at 1% of total power. Isointensity line key shown at base of *C*.

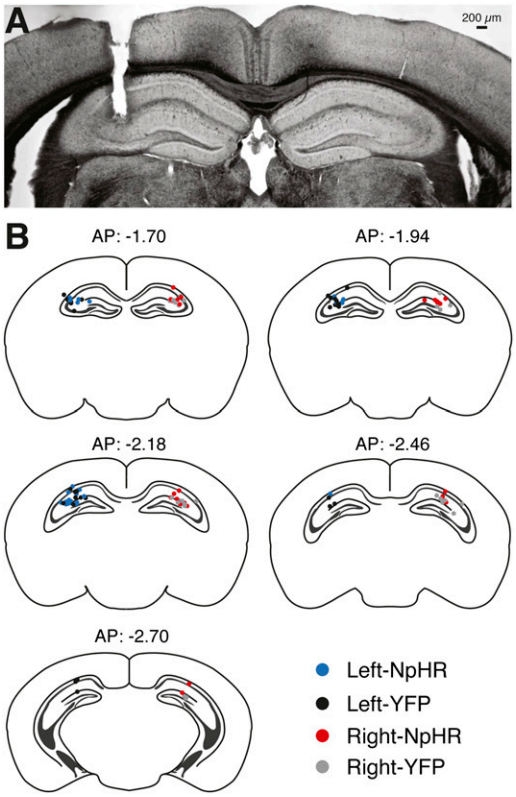

Fig. S2. Implant placement does not vary between behavioral groups. Posttesting, brains were fixed and sliced, and the placement of the deepest point of the implant was recorded for each mouse. (*A*) Representative brightfield image of implant site over left CA3. (*B*) The approximate locations of the fiber optic implant tip for each animal.